Hall, K. R., and L. Yarborough, "New Simple Correlation for Predicting Critical Volume," *Chem. Eng.*, **78**, 76 (1971).
Hildebrand, J. H., and R. L. Scott, *The Solubility of Nonelectrolytes*, 3rd ed., Reinhold Publishing Corp., New York (1950).
Hildebrand, J. H., J. M. Prausnitz, and R. L. Scott, *Regular Solutions: The Solubility of Gases, Liquids, and Solids*, Van Nostrand Reinhold Co., New York (1970).
Kessler, M. G., and B. I. Lee, "Improve Prediction of Enthalpy Fractions," *Hydrocarbon Processing*, **55**, 153 (1976).
Klink, A. E., H. Y. Cheh, and E. H. Amick, "The Vapor-Liquid Equilibrium of the Hydrogen-n-Butane System at Elevated Pressures," *AIChE J.*, **21**, 1142 (1975).
Lin, H. M., H. M. Sebastian, J. J. Simnick, and K. C. Chao, "Solubilities of Hydrogen and Methane in Coal Liquids," *Ind. Eng. Chem. Process. Design Develop.*, accepted for publication (1980).
Lyckman, R., C. A. Eckert, and J. M. Prausnitz, "Generalized Reference Fugacities for Phase Equilibrium Thermodynamics," *Chem. Eng. Sci.*, **20**, 685 (1965).
Nichols, W. B., H. H. Reamer, and B. H. Sage, "Volumetric and Phase Behavior in the Hydrogen-n-Hexane System," *AIChE J.*, **3**, 262 (1957).
Oliphant, J. L., H. M. Lin, and K. C. Chao, "Gas-Liquid Equilibrium in Hydrogen + Tetralin + Diphenylmethane and Hydrogen + Tetralin + m-xylene," *Fluid Phase Equil.*, **3**, 35 (1979).
Peter, S., and K. Rheinhartz, "Das Phasengleichgewicht in den Systemen H_2-n-Heptan, H_2-Methycycloxan and H_2-2,2,4 Trimethylpentan bei Loheren Drucken und Temperaturen," *Zeits. Phys. Chem.*, **24**, 103 (1960).
Prausnitz, J. M., and P. L. Chueh, *Computer Calculation for High Pressure Vapor Liquid Equilibria*, Prentice Hall, Englewood Cliffs, NJ (1968).
Redlich, O., and J. N. S. Kwong, "On the Thermodynamics of Solution," *Chem. Rev.*, **44**, 233 (1949).
Reid, R. C., J. M. Prausnitz, and T. K. Sherwood, *The Properties of Gases and Liquids*, 3rd ed., McGraw-Hill, NY (1977).
Sebastian, H. M., J. J. Simnick, H. M. Lin, and K. C. Chao, "Gas-Liquid Equilibrium in Mixtures of Hydrogen and Quinoline," *J. Chem. Eng. Data*, **23**, 305 (1978a).
Sebastian, H. M., J. J. Simnick, H. M. Lin, and K. C. Chao, "Gas-Liquid Equilibrium in Mixtures of Hydrogen and Thianaphthene," *Can. J. Chem. Eng.*, **56**, 743 (1978b).
Sebastian, H. M., J. J. Simnick, H. M. Lin, and K. C. Chao, "Gas-Liquid Equilibrium in the System Hydrogen + n-Decane at Elevated Temperatures and Pressures," *J. Chem. Eng. Data*, **25**, 68 (1980).
Sebastian, H. M., J. Yao, H. M. Lin, and K. C. Chao, "Gas-Liquid Equilibrium of the Hydrogen/Bicyclohexyl System at Elevated Temperatures and Pressures," *J. Chem. Eng. Data*, **23**, 167 (1978).
Simnick, J. J., C. C. Lawson, H. M. Lin, and K. C. Chao, "Vapor-Liquid Equilibrium of Hydrogen/Tetralin System at Elevated Temperatures and Pressures," *AIChE J.*, **23**, 469 (1977).
Simnick, J. J., K. D. Liu, H. M. Lin, and K. C. Chao, "Gas-Liquid Equilibrium in Mixtures of Hydrogen and Diphenylmethane," *I&EC Proc. Des. and Develop.*, **17**, 204 (1978).
Simnick, J. J., H. M. Sebastian, H. M. Lin, and K. C. Chao, "Solubility of Hydrogen in Toluene at Elevated Temperatures and Pressures," *J. Chem. Eng. Data*, **23**, 339 (1978).
Simnick, J. J., H. M. Sebastian, H. M. Lin, and K. C. Chao, "Gas-Liquid Equilibrium in Mixtures of Hydrogen + m-Xylene, and + m-Cresol," *J. Chem. Thermo.*, **11**, 331 (1979).
Yao, J., H. M. Sebastian, H. M. Lin, and K. C. Chao, "Gas-Liquid Equilibrium in Mixtures of Hydrogen and 1-Methylnaphthalene," *Fluid Phase Equil.*, **1**, 293 (1977/78).
Yen, L., and R. Alexander, "Estimation of Vapor and Liquid Enthalpies," *AIChE J.*, **11**, 334 (1965).

Manuscript received March 14, 1980; revision received July 2, and accepted July 9, 1980.

Simultaneous Measurement of Size and Velocity of Bubbles or Drops: A New Optical Technique

RAPHAEL SEMIAT
and
A. E. DUKLER
Department of Chemical Engineering
University of Houston
Houston, TX 77004

Accurate information on both the size and velocity of a dispersed phase is of importance to many problems in heat or mass transfer and reaction. Existing experimental methods are limited in their applicability, difficult to use, provide only size or velocity, and are of low statistical reliability. A new method is developed here which overcomes most of these shortcomings and permits accurate simultaneous measurement of the size and two dimensional velocity of the dispersed phase.

SCOPE

Knowing the size and velocity distribution of a dispersed phase is important to the prediction of heat and mass transfer as well as chemical reaction in many processes. Situations of industrial importance include spray absorbers, driers and combustors, bubble columns, thermosyphon reboilers, pipeline reactors, condensers operating in annular two-phase flow, as well as in spray cooling systems. Improvement in theoretical understanding of dispersed phase flows and transfer processes has been seriously limited by the paucity of reliable data by which to test new ideas. Thus, the objective of this research has been to devise a new method for making reliable simultaneous measurements of the size and velocity of two coordinate directions of the dispersed phase.

The earliest and still the most widely used methods of measurement are based on photography. Even with modern image analysis equipment and massive numbers of photographs, it is seldom possible to obtain statistically reliable data by photographic techniques except at great expense. Furthermore, two coordinate velocities are almost impossible to measure photographically.

The most recent methods for velocity are based on the use of crossed or reference laser beams and apply principles of laser doppler velocimetry. Measurement of velocity by this technique is well established as long as the dispersed-phase diameter is small enough to result in Mie scattering of the incident light. For air-water, this means drops or bubbles smaller than

Direct correspondence to A. E. Dukler. R. Semiat is currently with the Department of Nuclear Engineering, The Technion, Haifa, Israel.

0001-1541-81-4304-0148-$02.00.

150 μm. For most practical cases of interest in two-phase flow the diameters of interest are over 500 μm. Droplets in annular two-phase flow range up to 2,000 μm and, of course, bubble sizes of 5,000 μm are commonly observed. Satisfactory methods for simultaneous measurement of size with these crossed beam systems have yet to be reported.

In the new method presented here, a set of fringes is created in space using a laser beam passing through Ronchi gratings. Principles of geometric optics are used to measure velocities. Simultaneously, the time of passage of the drop or bubble through the beam is measured and combined with the velocity to find the diameter. Measurements are reported using this method to determine:

- the velocity and diameter of glass beads attached to the edge of a rotating disk;
- velocity of Taylor bubbles rising through a stagnant liquid;
- probability density distributions of the axial velocity and diameter of bubbles dispersed in a liquid flowing upward in a tube; and
- probability density distribution of axial and lateral velocity as well as size of droplets generated from a downward-directed flat fan type spray nozzle.

CONCLUSIONS AND SIGNIFICANCE

The principles of geometric optics have been successfully applied to the simultaneous measurement of velocity and diameter of bubbles or droplets in a variety of two-phase flow situations. The complication and limitation of crossed or reference beam systems can be eliminated by the use of Ronchi gratings which can be arranged in a simple manner to provide two coordinate velocities. A theoretical analysis of the technique provides definitive information on the maximum errors to be expected and these are shown to be very small.

PREVIOUS MEASUREMENT APPROACHES

The literature is rich in a variety of techniques for the measurement of the size of bubbles or drops. Azzopardi (1979) has presented a thorough review of sizing methods for drops making clear the limitations of each. Many are usable for bubbles as well. However, none of these methods is suitable for the simultaneous measurement of velocities and sizes under conditions characteristic of two-phase flow.

At low flow rates the velocity of large bubbles and drops have been measured by photography. These methods are limited to dilute dispersions where the field can be optically penetrated. For two-phase annular flow problems exist in obtaining optical access through the wall film. Furthermore, problems with depth of field make it difficult to obtain local velocities and distributions across a diameter. With photographic methods, it is seldom possible to collect sufficient data to obtain statistical reliability.

The velocity of small drops and bubbles have been measured by a cross beam or reference beam laser velocimeter. However, these methods depend on the existence of Mie scattering which limits their diameter for an air-water system to less than about 150 μm, well below the size range of interest in two-phase flow.

The existence of the new optical techniques have stimulated the development of devices for the simultaneous measurement of velocity and size. Fristram et al. (1973), Farmer (1974, 1978), and Lee and Srinivasan (1978), each using droplets of 50 μm or less reported methods for simultaneous measurement of drop size and axial velocity for flow of a dispersion of drops in a pipe. Either crossed-beam or reference-beam laser systems were used. In all three studies, the determination of size depends in one way or another on the amplitude of the light scattered from the particle. However, the amplitude of scattered light depends on the exact point where the drop intersects the incident laser beam and the viewing angle. Since the intensity of the beam decays near its edges, special and not totally successful arrangements must be made to account for the nonuniform beam. Even if the method were suitable technically, it would not be applicable for the large sizes of drops and bubbles of concern in two-phase flow.

Durst and Zare (1975) described a technique for the simultaneous measurement of size and velocity of large particles. Their method is based on the refraction (for transparent particles) or reflection (for nontransparent ones) of two laser beams directed toward the particle. The fringe spacing which is observed depends on the particle size and curvature. By using two photodetectors they were able to find the phase lag between the two signals from the same particle which is related to the diameter. Their report showed good signals could be obtained from many particles, but they did not unambiguously establish the relationship between the velocity and size measurement. Furthermore, detection of radial velocity using this technique is exceptionally difficult as is the alignment problem.

Wigley (1977) made simultaneous measurements of size and velocity of drops by the use of a dual laser beam and two photomultiplier tubes. The rate of crossing of the fringes was detected in one photomultiplier tube and the time that the signal was interrupted as the drop crossed the laser beam measured in a second PM tube. This method is very sensitive to the local position of the particle, as it intersects the beam with chord lengths rather than diameter being measured. As a result, the size information is ambiguous. The method also neglects the effect of velocity in other than the principal flow direction.

Hacker and Hussein (1978) measured size and velocity of large Taylor-type bubbles rising in a stagnant liquid. Two laser beams were directed across the diameter at two axial positions. The time for a bubble to successively intersect the two beams provided the velocity, while the time of passage across one beam gave information which combined with velocity made it possible to calculate the length. This simple approach is possible only for bubbles of the Taylor type which occupy almost the entire tube flow area.

The new technique presented here appears to resolve many of the difficulties of earlier methods. In addition, it permits simultaneous measurement of two coordinate velocities along with the diameter.

NEW OPTICAL TECHNIQUE FOR SIMULTANEOUS MEASUREMENT

The use of cross- or reference-laser beam techniques to measure velocity by Mie scattering is now a well-developed art. This phenomenon which is most useful for particles below 150 μm in diameter can be readily explained by the fact that when two laser beams are crossed, a field is formed containing dark and light fringes whose spacing can be precisely calculated from the frequency of the laser light and the angle between the two beams.

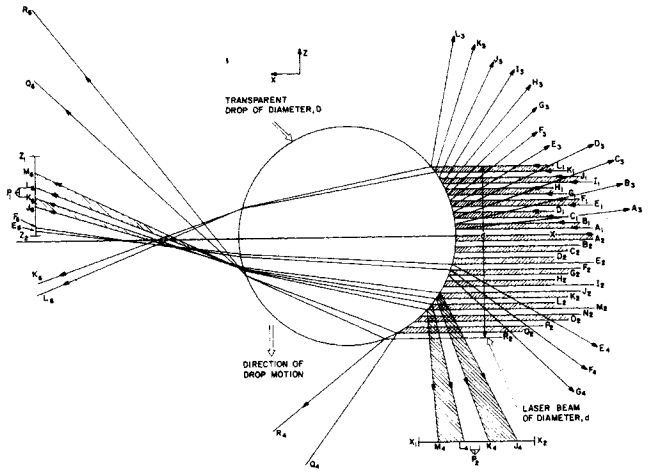

Figure 1. Geometric optics for a laser beam intersecting a drop.

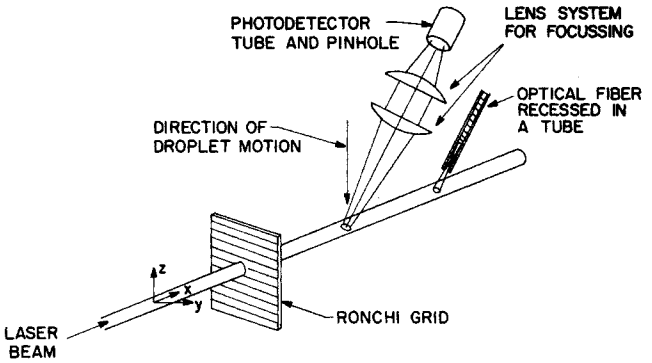

Figure 2. Arrangement for measuring one dimensional velocity component.

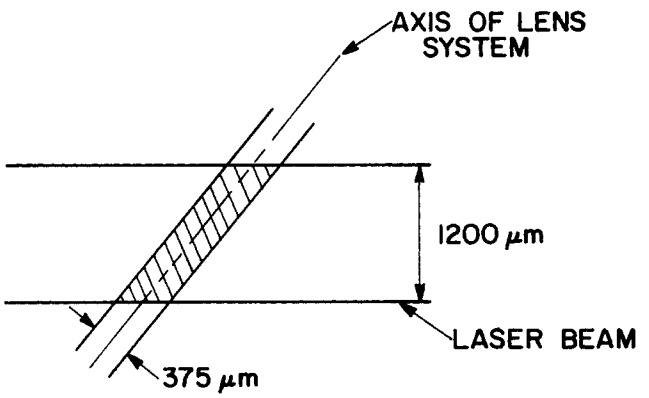

Figure 3. Optical sample space.

As a small particle crosses these fringes, the scattered light alternates in intensity between bright and dark as a fringe is crossed. The output of a PM tube, suitably located to collect the scattered light, will vary in amplitude depending on the particle size, angle of collection, and the portion of the laser beam intersected. The frequency of this signal is unambiguously related to the velocity at which the particle crosses normal to the array of fringes. This method depends on the existence of the Mie scattering phenomenon. For larger particles, the phenomenon of geometric optics comes into play where the particle itself acts as a lens exhibiting refraction and reflection phenomena.

Laser beams crossing over a large transparent particle result in the beams changing in direction because of refraction. The result is that the optical sample volume itself can change in position and size as can the fringe spacing. Thus, there is a basic weakness in using crossed-beam methods for measuring velocity of large particles. A second problem with this technique is to adapt it to the simultaneous measurement of size.

Eliminating Crossed Laser Beam Fringe System

The method starts with a suggestion by Ballik and Chan (1973, 1975) to replace the crossed-beam laser system with a Ronchi grating to generate the fringes in space. These gratings, which are widely used in optical laboratories, are very precisely ruled alternating transparent and opaque gratings set on film or glass. They are readily available at low cost in a wide variety of grating widths. Any light, even noncoherent white light, passed through the Ronchi grating will produce a continuous series of parallel planes of alternating dark and light spaces on the other side of the grating. If a laser beam is used as the light source, the spacing between the planes will be unambiguously related to that on the grating itself as will be explained below. Thus, the complexities inherent in locating two laser beams at an angle suitable to give the required fringe spacing, direction and optical sample space size are eliminated. The optical sample space size is fixed by depth of field and size of the lens system collecting the light or by the intersection of the viewing angle of an optical fiber and the laser beam.

GEOMETRIC OPTICS

Figure 1 is a ray diagram of a laser beam of diameter d having passed through a ronchi grid and being intercepted by a transparent water droplet of diameter D. The drop is moving downward in the direction indicated by the arrow. At the right of the drop is shown the laser beam. The axis of the laser beam is indicated as x. The edges of the light and dark planes on either side of the axis are designated as lines A_1, A_2, B_1, B_2, C_1, C_2, etc. Consider an instant, t, when the drop is located as shown relative to the beam. Follow the rays K_2 and L_2 which delineate a plane of light, as they intercept the surface of the drop as shown. Part of the light is reflected into beams K_4 and L_4, while part is bent into the drop and is refracted again as it leaves the surface at the other side, as indicated by K_6 and L_6. If a white screen were located at the plane $z_1 - z_2$, one would observe on this screen at time, t, an array of light and dark fringes delineated by the intersection of rays $E_6 - M_6$.

Now consider the movement of the drop downward. Because the axis of the laser beam remains unchanged and because the surface is translated downward, one would observe the fringes move across the $z_1 - z_2$ plane at exactly the same frequency at which they are intercepted by the drop as it falls through the laser beam. If a pinhole and photodetector were located at P_1, the output of the detector would be a voltage having a frequency equal to the fringe spacing of the laser beam divided by the unknown velocity. Thus, it is seen that refracted light generated by a large drop moving through a laser beam which has been moderated by a ronchi grating produces a signal similar to that of a crossed-laser beam useful for small drop sizes.

A similar result can be obtained by locating the photodetector to pick up reflections. Consider incident rays K_2 and L_2 as before. These rays are reflected downward and to the right, L_4 and K_4 as shown in Figure 1 as are those of adjacent rays. As the drop moves downward, the rays are displaced to the left and regions that were light become dark, then light again, etc. A pinhole and photodetector located at P_2 will pick up a time varying signal from which the velocity can be calculated. Note that at P_1, the angle enclosing the lighted fringe is smaller than that enclosing the reflected beam at P_2. Thus, the signal strength is greater at 1 than 2. Since this angle decreases with increasing drop size, it can be deduced that the signal strength increases with increasing droplet size. This result is the opposite of that observed as the drop size increases with Mie scattering in the crossed-beam method.

The particle does not need to be spherical for this technique to work. It is necessary only that the drop have a closed continuous surface and that the rate of change of the local radius of

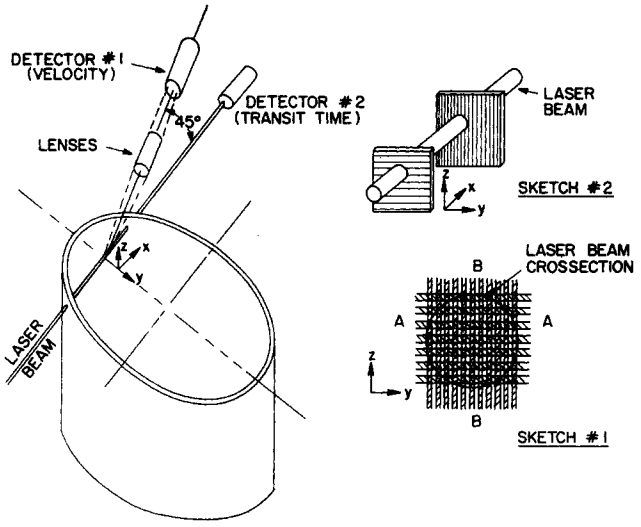

Figure 4. A system for measuring two coordinate velocities.

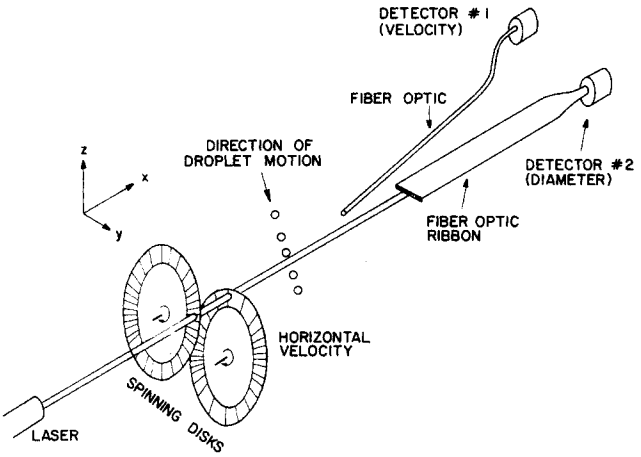

Figure 5. The use of spinning ronchi gratings.

curvature as it moves through the beam be small compared to the velocity.

When a bubble of diameter D replaces the drop in Figure 1, the reflected beams are similarly located. However, because of the inversion of refractive index, the rays diverge as they enter the bubble (rather than converging as shown in Figure 1) and diverge again as they re-enter the liquid. The end result of the same, and a PM tube located at 1 or 2 will detect fringe passing frequency.

Location and Effect of Photodetector on Sample Volume

In a conventional LDV system, the size of the optical sample space depends on the volume defined by the intersection of the two laser beams. This in turn depends on the diameter of the beams and the angle set between the two beams to obtain the desired fringe spacing. For the small angles required to obtain the wide fringe spacing needed for large drops, these optical sampling lengths are usually quite large, of the order of 5 mm or more. The position of the photodetector is unrelated to the size of the sample space and is usually located to maximize the signal intensity.

For the system proposed here, the sample volume is determined by the intersection of the laser beam and the optical line of sight of a detector through a lens system. Consider the arrangement shown in Figure 2. The axis of the photodetector is at 45° to the laser. The detector is fitted with a 250-μm pinhole. The lens focal lengths are such that the pinhole image at the focal plane is magnified by a factor of 1.5. Thus, the plane of the laser beam is intersected by a cone, the smallest dimension of which is

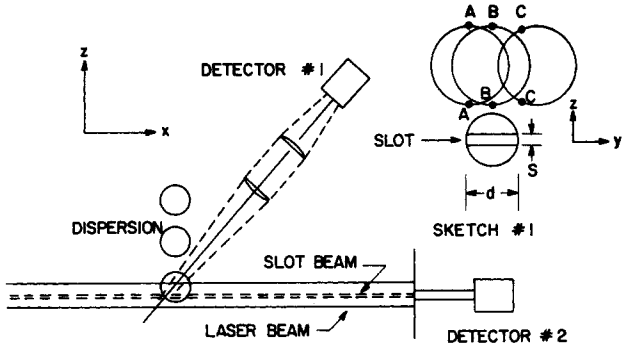

Figure 6. Configuration for velocity and size measurement.

375 μ, Figure 3. For the lenses selected, the divergence angle of the cone appears as parallel lines over the short distance of 1200 μm. Thus, the optical sample space from which a signal will be collected is a narrow strip 375 μm wide cut from a cylinder 1200 μm in diameter. For drops greater than 375 μ in diameter, the optical sample size is the drop size itself, clearly the smallest possible space which includes the drop.

Lens systems must be located outside of the flow field. In instances of dense dispersions, it is convenient to use fiber optics of small diameter to penetrate the field. By using small diameter fibers recessed in a tube, Figure 2, it is possible to define very small optical sample spaces.

Simultaneous Measurement of Axial and Radial Velocities

Consider the system shown to the left of Figure 4. A laser beam penetrates the pipe wall through a rod with optically polished ends. The pickup system is arranged to detect signal at the radial location either with externally located lenses or with an optical fiber located internally. Before entering the test section the beam passes through a ronchi grating located in the z-y plane. If the rulings are oriented horizontally, shown as A-A in sketch #1, the velocity measured will be axial. With a vertical orientation as in B-B the radial velocity can be measured.

Both velocities can be measured using a single photodetector. Locate two ronchi gratings as shown in sketch #2. The fringe spacing pair is selected so that two distinct and nonoverlapping frequencies are created as the particle moves through the sample space. Then, the two frequencies can be extracted by frequency filtering the signal from the detector. In many cases, this nonoverlapping feature is difficult to arrange with stationary gratings. However, either or both of the gratings can be prepared as an array of radial lines on a disk and rotated at a controlled speed through the laser beam creating a fixed and known frequency. In this way, the direction of the drop can be determined, a matter of importance for radial motion of the drops. Figure 5 is a sketch of the spinning ronchi disk arrangement used in this work. Detector #1 senses the two frequencies which characterize the z and y component velocities. Detector #2 is used to determine diameter as discussed below.

SIMULTANEOUS MEASUREMENT OF DIAMETER OF DISPERSED PHASE

Figure 6 is a view of the laser beam in the x-z plane. Photodetector #1 focuses on the optical sample space and detects the velocities by measuring the frequency of fringe crossing as discussed above. A narrow slot (in these experiments of 75 μm wide) and the full width of the laser beam is located in the z-y plane as shown facing into the beam. The projection of this slot along the axis of the laser beam is designated as the slot beam. This slot is fitted with a ribbon of optical fibers which conduct light to photodetector #2 located outside of the flow field. As a droplet passes across the slot beam, the light is refracted away from the optical fibers and the output signal from detector #2 drops. After the drop completes its passage, the signal intensity is restored. The signal from detector #2 is processed to calculate

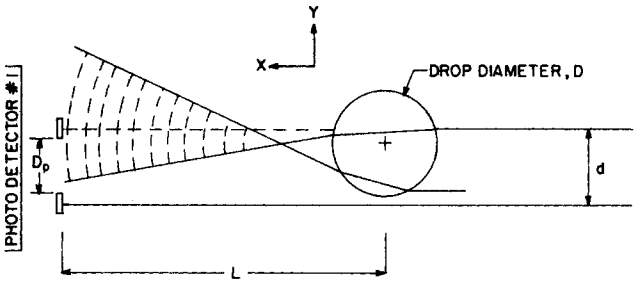

CASE A. CENTER OF DROP INSIDE OF LASER BEAM

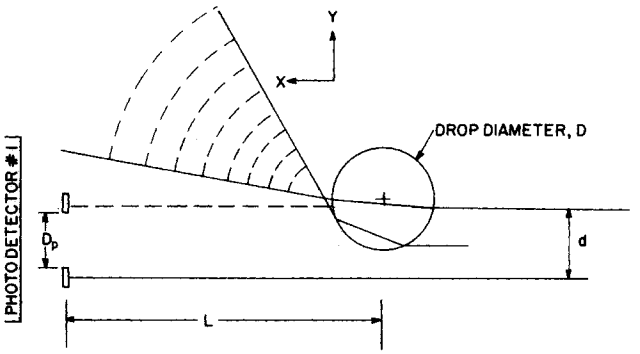

CASE B. CENTER OF DROP OUTSIDE OF LASER BEAM

Figure 7. Effect of drop location.

the passage time, τ. The diameter and velocities are related through the measured passage time. This passage time is:

$$\tau = \frac{D + s}{\vec{U}\cos[\arctan(U_y/U_z)]} \tag{1}$$

where

$$\vec{U} = U_y^2 + U_z^2$$

For situations where $U_y \ll U_z$, then

$$\tau = \frac{D + s}{U_z} \tag{2}$$

A drop which intersects the laser beam at any position along the beam will block the light and indicate a passage time, τ, from photodetector #2. However, within known error, only those droplets whose centers pass through the optical sample space will produce a simultaneous velocity signal. Recording of these two outputs and the use of relatively simple logic make it possible to reject passage time data except those simultaneously observed by the two detectors.

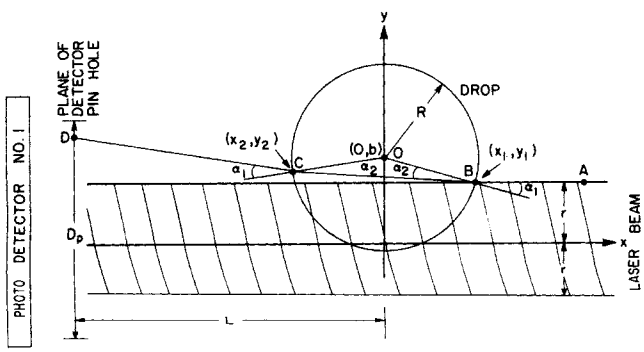

Figure 8. Geometric optics for calculating error in drop diameter.

Error Due to Chord vs. Diameter Measurement

Any method that attempts to measure diameter from a time of crossing measurement must face the problem that the chord rather than the diameter may pass through the sample space. While earlier methods have been unable to make this distinction, this method automatically does so. Refer to sketch #1 in Figure 6. Shown there in the z-y plane (not to scale) is a view of the laser beam of diameter, d, the slot beam of width, s, and a spherical droplet (or bubble) with diameter, D. The dispersion (in this case, drops) which is shown moving downward in the z direction, is indicated in three representative locations.

For drops located at A or B, the time that the slot beam interrupts is related to the distances A-A or B-B, both being the diameter of the drop. At location C, the interrupt time is determined by the chord length, C-C. However, for this location no velocity signal will be observed at photodetector #1, because the curvature of the drop in the z-y plane causes refraction sufficient to miss the pinhole in front of the detector. This is illustrated in Figure 7, which is a ray diagram drawn in the x-y plane looking down on two water drops as they move up through the beam in the z direction. In Case A, a drop of diameter, D, is located so that its center is just within the laser beam of diameter, d. Photodetector #1 which provides the velocity information is protected by a pinhole aperture of diameter, D_p, which is located a distance, L, in the x direction from the centerline of the drop.

From the ray diagram, it is evident that some of the refracted light will overlay the aperture opening and a velocity signal will appear. When the drop center is located outside of the laser beam as shown in Case B, it is equally clear that the limiting rays define a region that will not overlay the aperture opening. However, one can conceive of an aperture size large enough and a distance, L, small enough that a drop with its center located outside the incident beam could produce light through the aperture. In the case of a vapor bubble, the rays refract away from the bubble center increasing this possibility. Given D, D_p, d, and L and the refractive indices of the two phases, the principles of geometric optics can be used to calculate the limiting location of the center of the drop in the y direction which will result in light appearing in the photodetector. Once that position is located, the chord length created by the intersection with the laser beam can be calculated and the maximum possible error in the measured diameter determined.

Figure 8 is a view in the x-y plane of a drop whose center is located outside the laser beam, as it passes in the z direction through the beam. The origin is located so that the centerline of the laser beam lies along the x axis and the center of the particle lies on the y axis at a location $(0, b)$ where:

$$Z = \frac{b - r}{R} > 0$$

so that we are concerned only with drops whose centers are located outside the beam diameter. Photodetector #1 which provides the velocity information is located at a distance $x = -L$ and is protected by a pinhole of diameter, D_p. The limiting ray is the one at $y = r$ which intersects the drop; that is, if this ray, when it passes through the drop, refracts in such a way that it passes through the pinhole, signal will be received in velocity detector #1. If this ray does not enter the pinhole, no other ray within the laser beam (where $y < r$) will be captured within the pinhole. If the limiting ray enters the pinhole, there will be detection of velocity and the apparent drop diameter as calculated from Eq. 1 will be $2x_1$, rather than $2R$. Since,

$$x_1 = [R^2 - (b - r)^2]^{\frac{1}{2}} = (1 - Z^2)^{\frac{1}{2}} R \tag{4}$$

then the maximum possible error in the measured diameter is:

$$\epsilon = \frac{R - x_1}{R} = 1 - (1 - Z^2)^{\frac{1}{2}} \tag{5}$$

The ray located at $x = r$ is shown in Figure 8 as ABCD. The required relationship can be obtained by finding the equation

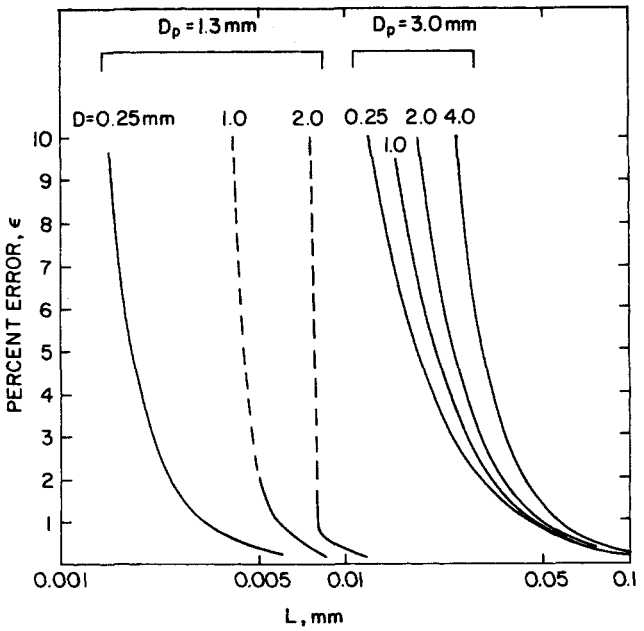

Figure 9. Maximum error in measured diameter: water drops in air (laser beam dia. = 1.2 mm).

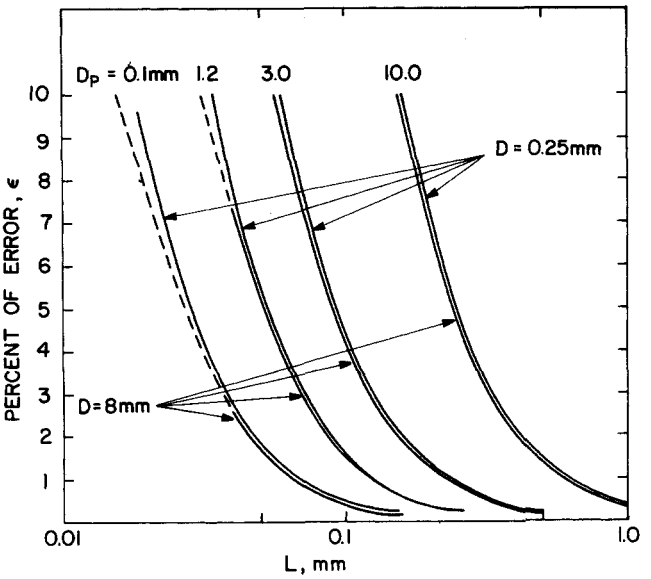

Figure 10. Maximum error in measured diameter: air bubbles in water (laser beam dia. = 1.2 mm).

for the line CD and setting $x = L$ and $y = D_p/2$ which indicates that the limiting ray just enters the pinhole. Then, one can find the value of x_1 or Z at which this takes place and through Eq. 5, the maximum error.

The slope of the CD line is:

$$M_3 = \tan(-\alpha_1 + \arctan M_2) = \frac{(D_p/2) - y_2}{-L - x_2} \tag{6}$$

Now, one must find α_1, M_2, y_2 and x_2. The boundaries of the laser beam are described by the line equation, $y = \pm r$, and the sphere by $(y - b)^2 + x^2 = R^2$.

Consider the ray, AB. The angle, α, made with the normal is equal to arc tan M_1 where M_1 is the slope of the normal, OB. But:

$$M_1 = -\frac{b - r}{x_1} = -\frac{Z}{1 - Z^2} \tag{7}$$

and

$$\alpha_1 = \arctan \frac{Z}{1 - Z^2} \tag{8}$$

The angles α_1 and α_2 are related through Snell's law, $n_1 \sin\alpha_1 = n_2 \sin\alpha_2$. For drops in air $n_1 = 1.0$ and $n_2 = 1.33$, while for bubbles in water $n_1 = 1.33$ and $n_2 = 1.0$. Thus,

$$\alpha_2 = \arcsin\left(\frac{n_1}{n_2} \sin\alpha_1\right) \tag{9}$$

Taking the line integral from B to C and recognizing that this arc length equals $(\pi - 2\alpha_2)R$ permits the determination of x_2.

$$(\pi - 2\alpha_2)R = -\int_{x_1}^{x_2}\left[1 - \left(\frac{dy}{dx}\right)^2\right]^{\frac{1}{2}} dx \tag{10}$$

Solving gives,

$$x_2 = R\sin[-(\pi - 2\alpha_2) + \arcsin(1 - Z^2)^{\frac{1}{2}}] \tag{11}$$

From the equation for the sphere,

$$y_2 = R\left\{\left[Z + \frac{r}{R}\right] - \left[1 - \left(\frac{x_2}{R}\right)^2\right]^{\frac{1}{2}}\right\} \tag{12}$$

M_2, the slope of the line CO, is found from its definition,

$$M_2 = \frac{\left(Z + \frac{r}{R}\right)R - y_2}{-x_2} \tag{13}$$

Now it is possible to relate the error to the system orientation as follows:

- Given Z the error, ϵ, can be found from Eq. 5 and α_1 from Eq. 8.
- For the fluid properties and dispersion of interest (drops/bubbles), n_1 and n_2 are specified and Eq. 9 is used to find α_2.
- Find x_2 from Eq. 11 for any drop radius, R.
- Find y_2 from Eq. 12 since the laser beam radius, r, is specified.
- Find M_2 from Eq. 13.
- Finally, for any D_p, find the distance L from Eq. 6. Any detector pinhole located at a distance greater than L will give an error less than ϵ.

These calculations have been carried out for water drops in air and bubbles in water using a laser beam with diameter of 1.2 mm, as used in this work. The results appear in Figures 9 and 10 for the range of variables of interest. Note that if the pinhole diameter is no larger than the laser beam, or if $D_p \leq d$, the error for drops is always zero. The dotted portion of the curves represent distance, L, so small that the pinhole plane is located within the drop or bubble, an obvious impossibility. It is clear that for

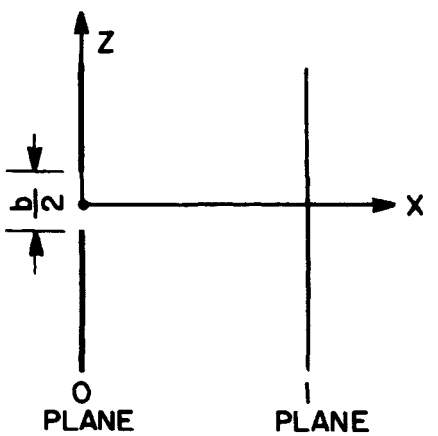

Figure 11. Analysis of images created by a laser beam downstream of a slit.

drops the error is readily made very small even if pinholes are used larger than the laser beam. For bubbles somewhat greater errors can be expected but if a pinhole is used of the laser beam diameter and the sample space is located a distance at least 20 mm from the detector, the error is less than 1%.

Error Due to Multiple Particles in Slot Beam

For high concentration of dispersion, a drop or bubble can enter the slot beam before an earlier one has completed its passage giving an erroneous passage time and an error in diameter. The probability of this error can be obtained by recognizing that the process of drop or bubble passage is a Poisson process and that for such a process the probability density of the time between arrival of successive particles is (Papoulis, 1965):

$$p(t_a) = n_p \exp(-n_p t_a) \tag{14}$$

n_p is the average rate at which particles pass through the slot beam, in the z direction (for which velocity is simultaneously detected) and t_a is the time between successive arrivals in the beam. Multiple particles exist, when $t_a < \tau$, that is, when the arrival time between successive particles, t_a, is less than the passage time for a particle to move across the slot beam, τ. The probability of this event is given by:

$$P(t_a < \tau) = \int_0^\tau n_p e^{-n_p t a}\, dt_a = 1 - e^{-n_p \tau} \tag{15}$$

It is a simple matter to measure n_p during the experiment. For purposes of experimental design, an upper limit estimate of n_p can be obtained by assuming that the dispersed phase of diameter, D, having a known flow rate or superficial velocity, U_D^s, is uniformly distributed over the flow area and the rate at which particles cross the slot beam is in the ratio of the area of the slot beam to that of the tube flow area. Then,

$$n_p = \frac{6U_D^s ld}{\pi D^3} \tag{16}$$

Here l and d are the length of the slot beam and the diameter of the laser beam respectively. Using Eq. 2 for τ gives:

$$n_p \tau = \frac{6ld(D + s)}{\pi D^3} \frac{U_D^s}{U_z} \tag{17}$$

This procedure will heavily overestimate the probability for error, since the fraction of particles for which both velocity and transit time are simultaneously detected is small. In the experiments reported below, the measured n_p was less than 10% of that calculated from Eq. 16.

FRINGE IMAGES CREATED BY A GRATING

When an optical grating is illuminated with coherent light, exact images of the grating are formed at finite distances from the grating. If b is fringe spacing on the grating and λ is the wavelength, for $(\lambda/b)^2 << 1$, Lord Rayleigh (1881) showed that these exact images, called Fourier images, are spaced at distances behind the grating:

$$S_n = n\left(\frac{2b^2}{\lambda}\right) = nS \quad n = 1, 2, 3, \ldots \tag{18}$$

where $S = 2b^2/\lambda$ is the image periodicity. Between these Fourier image planes, many other images appear. These are called Fresnel images and are also periodic, but do not necessarily carry only the periodicity of the grating. Because this method depends on knowing the fringe spacing in order to calculate the velocity of the particle traversing the beam, it is necessary to understand how this spacing can vary for images at all positions from the grating along the beam.

Consider the slit of width $b/2$ whose length, a, is located in the y direction and in the $y - z$ plane. In Figure 11, the planar slit extends normal to the paper in the y direction.

The distribution of the field on plane 1 which is generated by perfectly collimated light entering the slit at $z = 0$ on plane 1 is:

$$\phi(z_1, y_1) = \frac{\exp(jkx)}{j\lambda x} \int_{-\frac{a}{2}}^{\frac{a}{2}} \int_{-\frac{b}{4}}^{\frac{b}{4}} \exp\left(j \frac{k}{2x} [(z_1 - z_0)^2 + (y_1 - y_0)^2]\right) dz_0 dy_0 \tag{19}$$

where z_1, y_1 are the coordinates of the image point of interest on the 1 plane and $k = 2\pi/\lambda$ is the wave number (Goodman, 1968). This expression can be separated into the product of two integrals:

$$\phi(z_1, y_1) = \frac{\exp(jkx)}{j\lambda x} \psi(z_1)\psi(y_1) \tag{20}$$

where

$$\psi(z_1) = \int_{-\frac{b}{4}}^{\frac{b}{4}} \exp\left[\frac{jk}{2x}(z_1 - z_0)^2\right] dz_0 \tag{21}$$

$$\phi(y_1) = \int_{-\frac{a}{2}}^{\frac{a}{2}} \exp\left[\frac{jk}{2x}(y_1 - y_0)^2\right] dy_0 \tag{22}$$

For multiple slits in one direction, say z, the second integral can be considered a constant, say $\psi(y_1)$. However, for the direction of multiple slits, the new integral ψ_N can be obtained by superposition.

$$\psi_N = \sum_{-N}^{N} \int_{(nb-\frac{b}{4})}^{(nb+\frac{b}{4})} \exp\left[j \frac{k}{2x}(z_1 - z_0)^2\right] dz_0 \tag{23}$$

Here $2N$ is the number of slits illuminated by the laser beam. Writing the exponential in trigonometric form and the variables in dimensionless form gives:

$$\psi_N^* = \sum_N^N \left[\int_{\eta_{n_1}}^{\eta_{n_2}} \left(\cos\frac{\pi}{2}\eta^2 d\eta + j\int_{\eta_1}^{\eta_2} \sin\frac{\pi}{2}\eta^2 d\eta\right)\right] \tag{24}$$

where

$$\eta = (z_1^* - z_0^*)/\sqrt{X^*} \qquad x^* = x/S = x\lambda/2b^2$$

$$\eta_{n_1} = \frac{n - (1/4) - z_1^*}{\sqrt{X^*}} \qquad z^* = z/b$$

$$\eta_{n_2} = \frac{n + (1/4) - z_1^*}{\sqrt{X^*}} \qquad \psi_N^* = \psi_N/\sqrt{x\lambda/2}$$

The integrals depend only on the limits. Designate the Fresnel integrals:

$$\int_{\eta_1}^{\eta_2} \cos\frac{\pi}{2}\eta^2 d\eta = [C(\eta_2) - C(\eta_1)]$$

$$\int_{\eta_1}^{\eta_2} \sin\frac{\pi}{2}\eta^2 d\eta = [S(\eta_2) - S(\eta_1)]$$

or

$$\psi_N^* = \sum_{-N}^{N} \{[C(\eta_{n_2}) - C(\eta_{n_1})] + j[S(\eta_{n_2}) - S(\eta_{n_1})]\} \tag{25}$$

The intensity of the manochromatic field is found from the modular value of the field distribution:

$$I(z_1, y_1) = |\phi(z_1, y_1)|^2 = \frac{1}{4} |\psi_N(z_1)|^2 \cdot |\psi(y_1)|^2 \tag{26}$$

Since $\psi(y_1)$ does not depend on z_1 and since the interest is in the distribution of intensity, not its magnitude, we define an intensity at z as:

$$I(z_1) = |\psi_N^*(z_1)|^2 = \sum_{-N}^{N} [C(\eta_{n_2}) - C(\eta_{n_1})]^2 + [S(\eta_{n_2}) - S(\eta_{n_1})]^2 \tag{27}$$

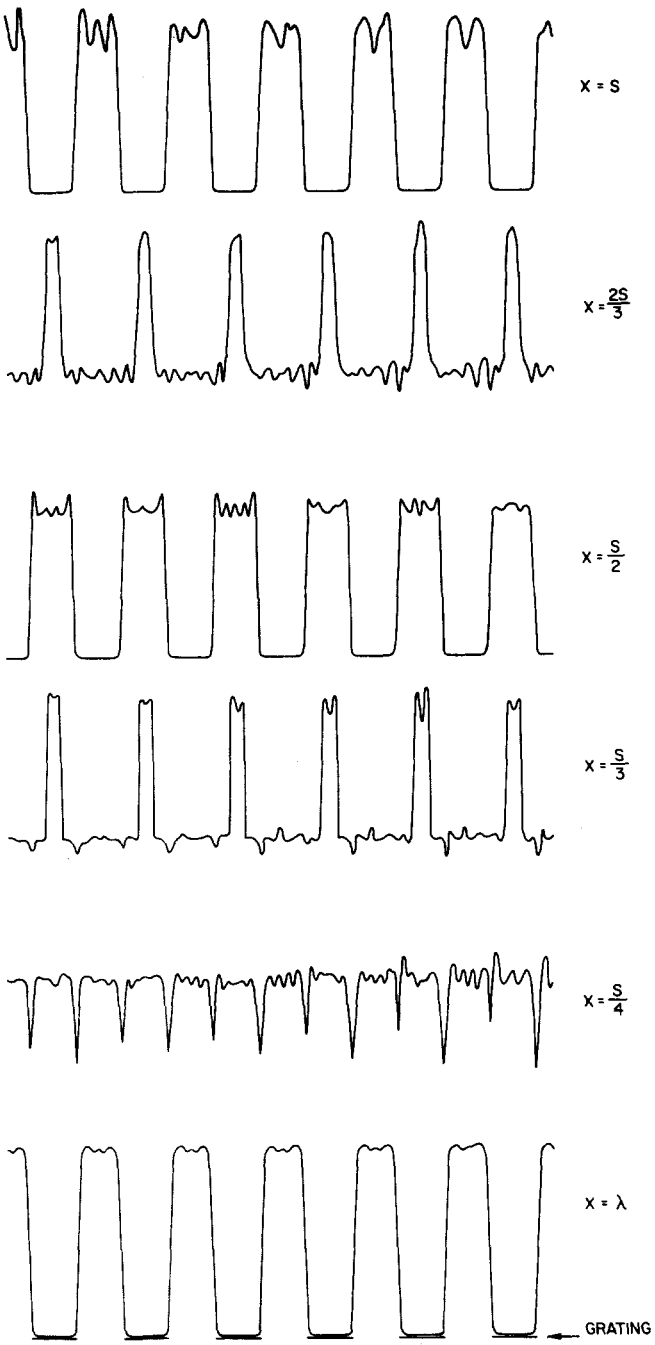

Figure 12. Fresnel and fourier image behind a grating, $0 < X \leq S$.

Eq. 27 gives the intensity distribution at each x plane, once N is known. Numerical solution can reveal the fringe pattern at all locations from the grating. This has been accomplished for the experimental system used here: grating of 200 lines/cm or $b = 50$ μm in diameter or $N = 12$. Figures 12 and 13 display the result. Figure 12 shows the fringe pattern at various locations between the grating and the first Fourier image at $X = S = 2b^2/\lambda$. At the bottom is shown the location of six opaque and transparent slits on the gratings. Each trace above shows the intensity distribution at a X location from the grating.

Note that one wavelength from the grating the fringe pattern is duplicated identically. At $X = S/4$, a fringe pattern appears which has precisely twice the frequency as the grating. Thus, a particle passing across the plane will "see" twice the frequency as well as the primary frequency. At $X = S/3$, $S/2$ and $2S/3$, fringe spacing is again identical to the grating but the intensities are inverted, and at $X = S$ the grating image is reproduced again. Although the fringe width and shape differ from that of the grating along X, the fringe spacing is the same at all locations except near $S/4$ or $3S/4$ where it is precisely doubled. Particles passing near these planes will cause signals in the photodetector which carry a frequency component twice that of the true value. Thus, it is necessary to incorporate frequency filtering in the circuit to reject the higher frequencies. In this way, the result will be independent of the Z plane through which the particle passes.

Image patterns for $X > S$ are displayed in Figure 13. The problem of half fringe spacing disappears as successive Fourier image locations are passed. Thus, at $X = 4.25S$ one sees double images only over the first five fringes, while at $X = 6.25S$ there are no double images. For these experiments $\lambda = 0.6328$ μm and thus $S \simeq 8$ mm. Thus, the double frequency will not appear, if the optical sample space is located at least 50 mm from the grating. Chan and Ballik (1974) comment that at large distances the Fourier images disappear and this is confirmed from the solution of the equations presented here. With these equations, it is now possible to compute the fringe pattern at all locations of interest for an experiment before preceding with the experimental setup. In this way, the suitable electronic filtering can be incorporated, the existence of correct fringe spacing verified, and thus avoid the laborious trial-and-error so often associated with these types of optical experiments.

Signal Processing System

Figure 14 is a schematic diagram of the signal processing system for measuring 2D velocity and size. The signal from

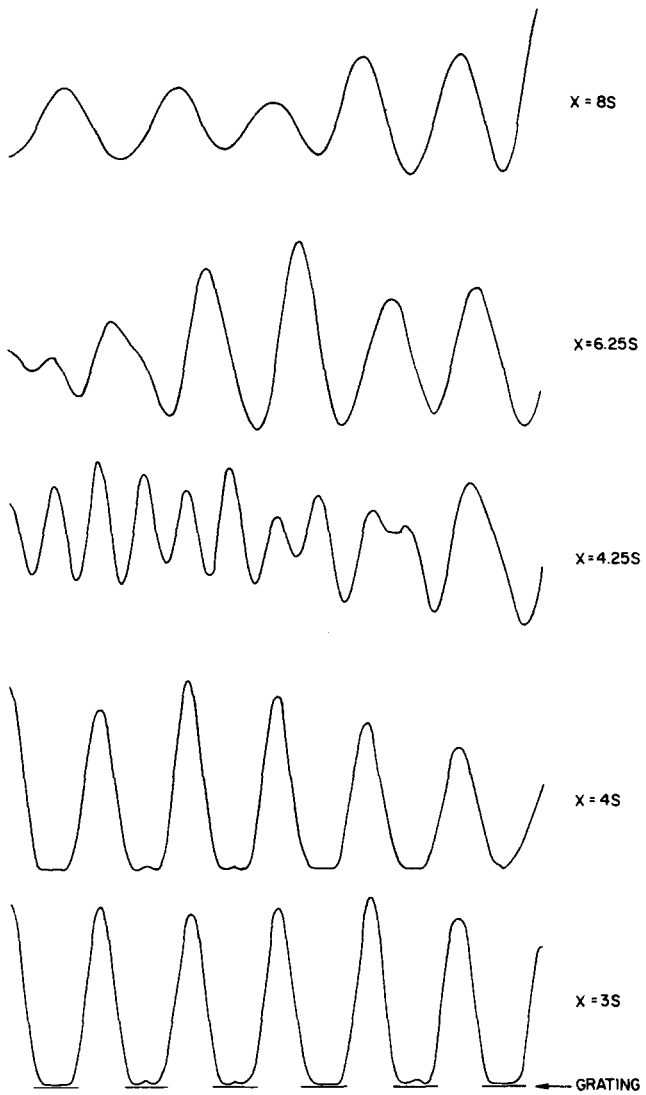

Figure 13. Fresnel and fourier images behind a grating, $X > S$.

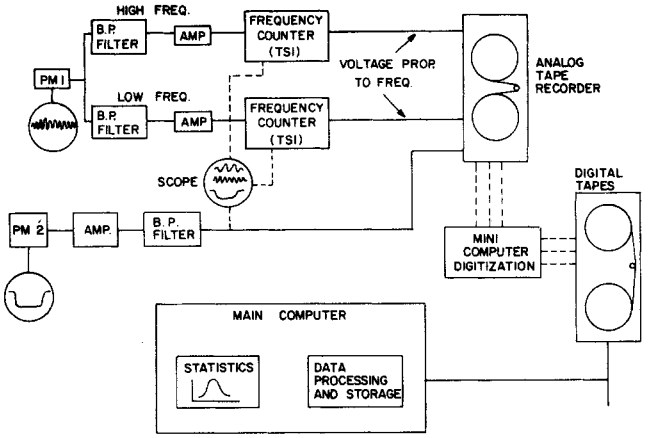

Figure 14. Signal processing system.

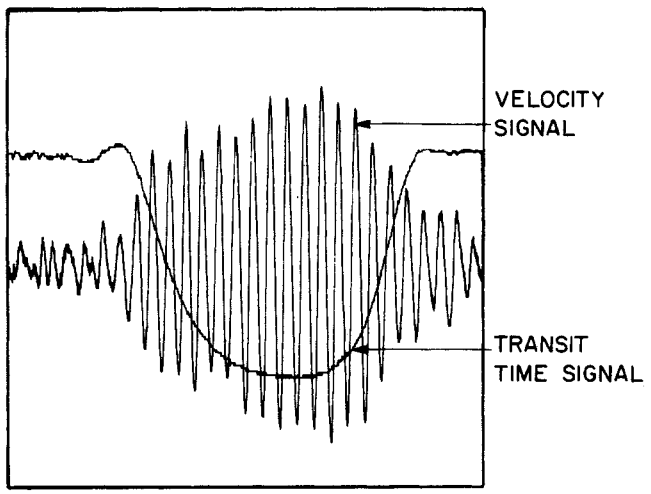

Figure 15. X-Y plot of output from photo detectors #1 & #2.

photomultiplier #1 is filtered to produce the two frequencies proportional to the two velocities of interest. After amplification, each is passed to a TSI Model 1990 counter-type velocimeter. This instrument detects the presence of a burst of light, measures the frequency in the burst and transduces this frequency into an output voltage proportional to frequency which is held until the next burst is detected. The two such voltages were recorded on two channels of an instrumentation quality FM tape recorder with the transit time recorded on a third channel. The analog signals from the three channels were digitized and stored on computer tape or disks for subsequent processing. Computer programs were prepared to calculate statistical quantities of interest such as the probability densities of the measured quantities, the various moments and the particle count.

TABLE 1. SIMULTANEOUS MEASUREMENT OF SIZE AND VELOCITY OF GLASS BEADS

Test		N*	Known Values	Measured Values	% Error	Std Deviation %
A	Velocity, cm/s	17	70.1	69.7	0.6	1.3
	Size, μm		802	797	0.7	1.2
B	Velocity, cm/s	10	70.5	69.9	0.8	0.9
	Size, μm		3248	3245	0.1	0.7
C	Velocity, cm/s	10	76.5	76.7	0.3	1.2
	Size, μm		5809	5823	0.3	1.3

*N = Number of Repeated Experiments.

Experimental Measurements

This technique was applied to a variety of measurements:

- Velocity and diameter of glass spheres attached to the edge of a disk which was rotated through the beam at a known velocity
- Velocity of Taylor bubbles rising through a stagnant liquid
- Axial velocity and diameter of bubbles dispersed in a liquid flowing upward in a vertical tube
- Velocity and size of drops in a flat spray.

In all of these experiments a 15-MW helium-neon laser was used having a beam diameter of 1.2 mm and a wavelength, λ = 0.6328 μm.

Velocity and Size of Glass Beads. A thin disk of known diameter was rotated with a constant speed motor. On the outer edge of the disk, a single glass sphere whose diameter was measured with an optical microscope was carefully attached to the edge of the disk with cement. The disk was then positioned so that with each revolution the sphere passed through the fringe system of the laser beam. These experiments used a ronchi grating having 200 lines per cm and the configuration was as shown in Figure 2. The output of the two photodetectors was displayed on the face of a dual-beam digital storage oscilloscope equipped with $x - y$ plotter output. A typical result is shown in Figure 15. The sine wave burst shows output from detector #1 and is used to calculate velocity. The second curve represents detector #2 which shows transit time through the beam.

Three glass beads having optically measured diameters of 5809, 3248 and 802 μm were tested. These optically measured diameters were accurate to approximately 10 μm. Comparisons between known and experimentally determined velocity and size were as shown in Table 1. In no case, was the error either in size or velocity greater than 1%.

Velocity of Taylor Bubbles. Taylor bubbles were generated by injecting known volumes of air into a 38-mm diameter vertical column of stagnant water. A large hypodermic syringe was used as the injector. This type of bubble occupies almost the entire cross-sectional area of the tube as it rises and its velocity for high surface tension fluids such as water has been shown (White et al., 1962) to be given by the equation, $U_{TB} = 0.35\sqrt{gD_T}$ where D_T is the tube diameter. Thus, in this case, a rise velocity of 0.213 m/s is to be expected. Experiments were made with a series of Taylor bubble sizes. These measurements were made with the laser beam passing across a diameter of the tube and the velocity photodetector focused at the centerline. A ronchi grating having 20 lines per mm was used. Velocity measurements were also made timing the bubble velocity between marked locations as recorded on movie film.

The comparisons for three bubble sizes are shown in Table 2. Agreement is seen to be excellent with the deviations somewhat greater for the smallest bubble size. For the smallest bubble volume, the diameter of the Taylor bubble becomes considerably smaller than the tube diameter and the bubble tends to oscillate. At these low translational velocities, the oscillatory motion is significant compared to the translational velocity and this method "sees" the sum of the two.

Velocity and Diameter of Dispersed Bubbles. The single beam laser system was used to measure the size and axial velocity of the dispersed phase during upward, two-phase bubbly flow in a vertical tube of 51-mm diameter. The laser beam was directed across the diameter after passing through a ronchi grating having 20 lines/mm. The slot beam was 250 μm wide. The velocity signal was collected by using an unshielded single optical fiber located so that it captured light from bubbles intersecting the beam at all locations along the diameter. Thus, the data collected for each flow condition represent bubble velocities and diameters averaged across the entire flow area. Signal processing was in accord with that shown in Figure 14, but with only one velocity being detected.

Experiments were carried out at a low superficial gas velocity of 9 mm/s over a wide range of liquid rates. Probability densities of the bubble velocity and diameter appear in Figures 16

TABLE 2. VELOCITY OF TAYLOR BUBBLES

Laser Measurement			Film Measurement		Deviations	
Bubble Volume	Number Bubbles Measured	Mean Velocity cm/s	Number Bubbles Measured	Mean Velocity cm/s	Laser to Equation	Laser to Film
20 cm^3	47	20.9 cm/s	13	20.7 cm/s	1.8%	1.0%
15	57	21.0	10	21.2	1.4%	1.0%
10	43	22.2	12	20.7	4.2%	7.2%

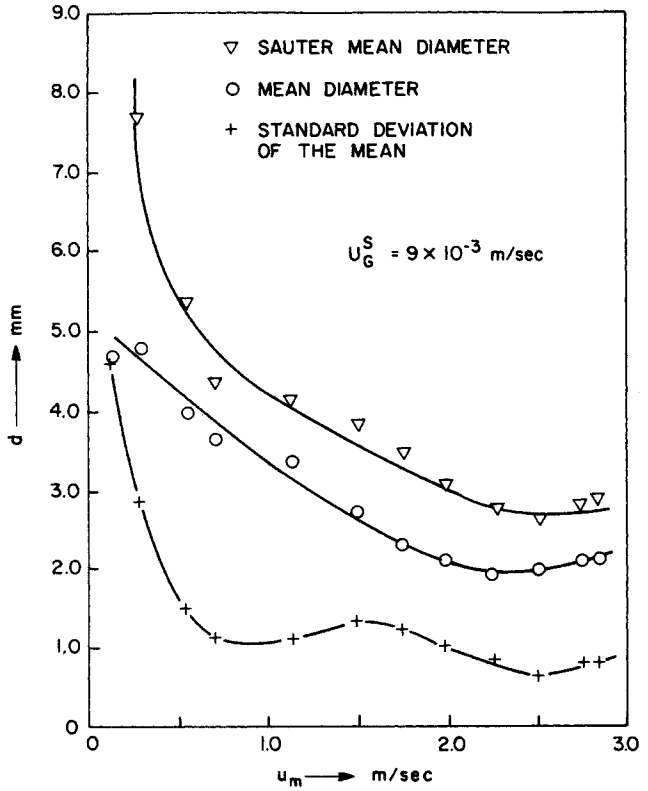

Figure 18. Mean values of diameter and velocity for upward bubble flow.

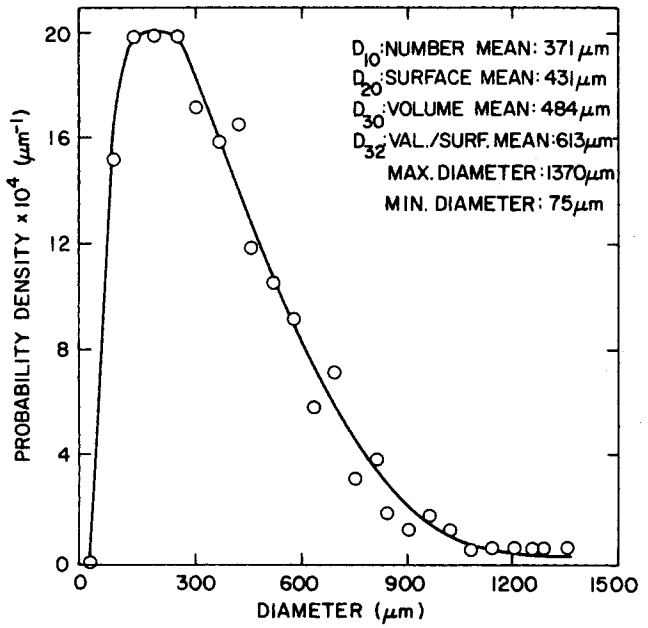

Figure 19. Spraying Systems Inc. nozzle 5004: probability density distribution of diameter.

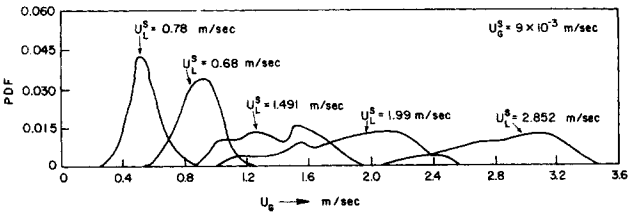

Figure 16. Probability density function of the bubble velocities.

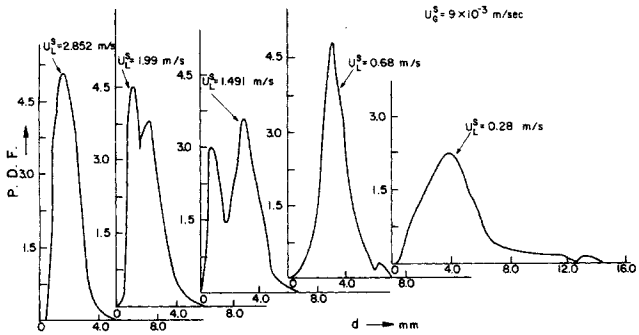

Figure 17. Probability density function of bubble diameter.

and 17. For each flow rate pair data were collected from 1000-2500 bubbles. This ability to take such large sample numbers is a significant benefit of the measuring method and assures good statistical reliability. The count can be extended indefinitely by using longer runs and reading times.

As an example of the type of data processing possible, Figure 18 shows the variation with two-phase velocity of the number

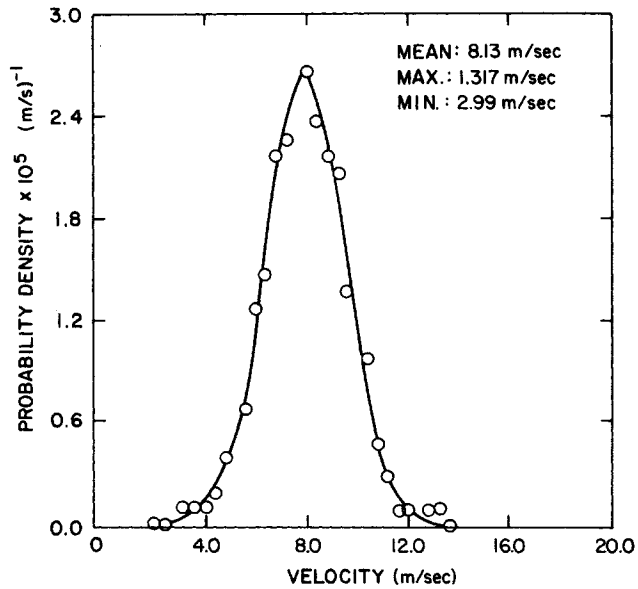

Figure 20. Spraying Systems Inc. nozzle 5004: probability density of vertical velocity.

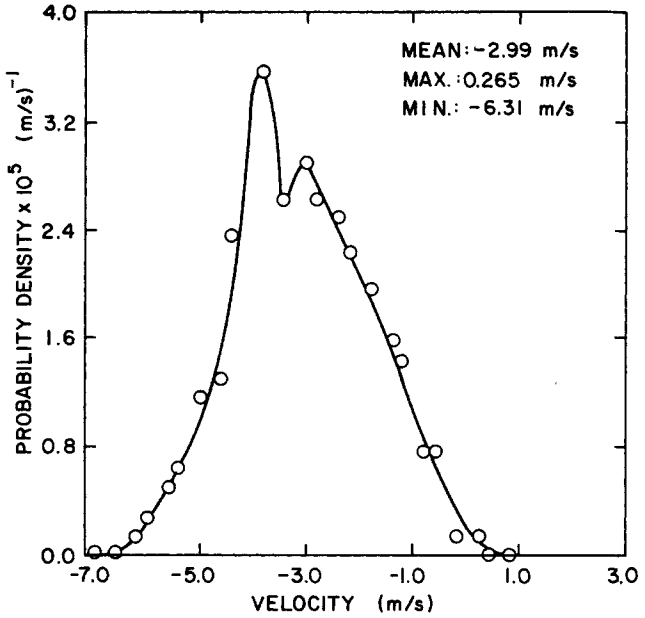

Figure 21. Spraying Systems Inc. nozzle 5004: probability density of lateral velocity.

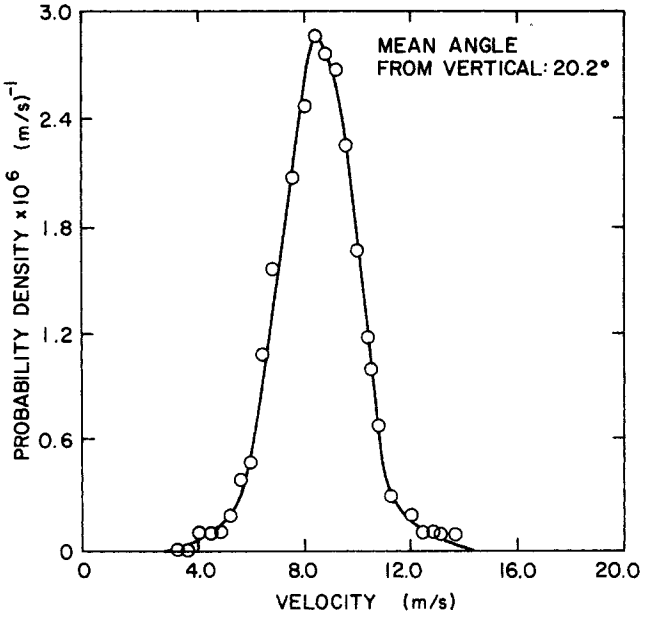

Figure 22. Spraying Systems Inc. nozzle 5004: probability density of resultant velocity.

mean and the Sauter mean diameters computed from the probability densities as well as the standard deviation of the number mean. From Figure 10, the diameter error due to chord measurement is seen to be zero. Using measured count rate of particles passing the slot beam and Eq. 15, the probability of multiple particles in the beam is less than 2%.

Velocity and Diameter of Drops in a Flat Spray. Two dimensional velocity and diameter were measured near the centerline of a flat water spray generated from a spray nozzle. A Spraying Systems Co. 50° Flat Spray Nozzle No. 5004 was used with an inlet pressure of 6.9×10^4 N/m^2. The spinning disk arrangement shown in Figure 5 was used to make simultaneous measurements of vertical and lateral velocity along the drop diameter. Each disk was 72.5 mm in outer diameter and contained 4096 radial lines resulting in fringe spacing of 50 μm. Frequency filtering, detection and data processing, Figure 14, was used and the software system was used to process the data. Thus, the full system, both hardware and software, was tested. The optical system was arranged to sample the flat spray over its entire thickness, in this case, about 28 mm.

Primary results are shown in Figures 19-21 where the probability densities are shown for diameter, vertical and lateral velocities, respectively. The probability density of the resultant velocity is shown in Figure 22 where the angle of this vector from the vertical is indicated. This run represents the processing of 1500 samples; thus, the statistical reliability of the data is reasonably high. The actual run time was less than 2 minutes. It is obvious that doubling or quadrupling the sample count would be relatively easy. Results with unmatched reliability can be obtained with run times of less than 10 minutes. Note also that the lateral velocities detected included both negative (inward toward the axis) as well as positive lateral velocities as is to be expected in such a spray. The probability of error in diameter due to multiple particle detection is less than 0.5%.

A comparison is shown in Figure 23 of the cumulative volume distribution determined by this method with that obtained by the nozzle manufacturer, the Spraying Systems Inc. Data were obtained photographically by the use of high intensity ultrashort duration flash and image analysis techniques applied to the photographs. The agreement is seen to be excellent.

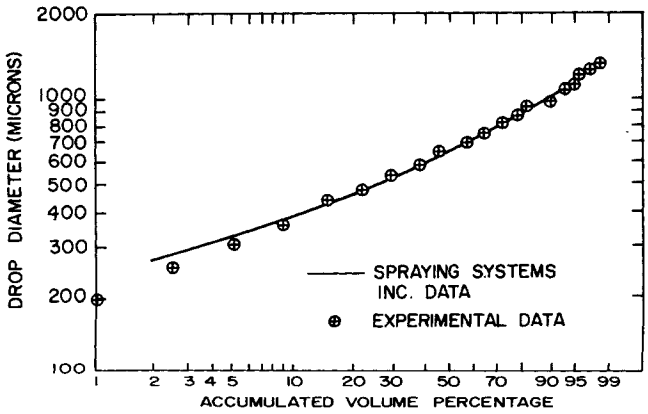

Figure 23. Particle size distribution Spraying Systems Inc. 50° flat spray nozzle No. 5004 @6.9×10^4 N/m^2.

ACKNOWLEDGMENT

The support of the U.S. Nuclear Regulatory Commission made this work possible.

NOTATION

a	=	slit depth in y direction
b	=	fringe spacing on the grating
d	=	laser beam diameter
D	=	particle diameter
D_p	=	pinhole diameter
D_T	=	tube diameter
g	=	acceleration of gravity
I	=	light intensity
k	=	wave number
l	=	length of laser beam in fluid between source and detector
L	=	distance between photodetector and particle center in x direction
n	=	refractive index
n_p	=	average rate of particles passing through laser beam
N	=	half the number of fringes illuminated by the laser beam
r	=	radius of the laser beam
R	=	radius of the particle
s	=	width of the slot for the diameter signal
S	=	periodicity of the Fourier images

S_n = the nth distance of the Fourier image from the grating
t = time
t_a = time between successive arrivals of the dispersed phase at the laser
$\vec{U}$ = resultant velocity of the particle
U_y, U_z = velocity components in the y and z directions
U_{TB} = velocity of Taylor bubbles
U_D^s = superficial velocity of the dispersed phase
U_C^s = superficial velocity of the gas phase
Z = dimensionless distance from the center of the particle to the center of the laser beam
Z^* = dimensionless distance from the grating to the image plane

Greek Symbols

α = angle between light ray and the normal to particle interface
ϵ = maximum possible error in detecting particle chord as diameter
η = dimensionless slit distance
λ = wavelength
ϕ = distribution function for the light field
τ = transit time of the particle passing through slot beam

LITERATURE CITED

Azzopardi, B. J., "Measurement of Drop Sizes," Int. J. Heat and Mass Tr. **22**, 1245 (1979).

Ballic, E. A., and Chan, J. H. C., "Fringe Image Technique for the Measurement of Flow Velocities," *Appl. Optics*, **12**, 2603 (1973).

Chan, J. H. C., and Ballic, E. A., "SNR in Optical Velocimeters: Effect of Particle Number Density," *Appl. Optics*, **14**, 1839 (1975).

Chan, J. H. C., and Ballic, E. A., "Application of Fourier Images to the Measurement of Particle Velocities," *Appl. Optics*, **13**, 234 (1974).

Durst, F., and Zaré, M., "Laser Doppler Measurements in Two Phase Flows," *Proc. of the LDA-Symposium*, Copenhagen, 4-3-429 (1975).

Farmer, W. M., "Observations of Large Particles with a Laster Interferometer," *Appl. Optics*, **13**, 610 (1974).

Farmer, W. M., "Measurement of Particle Size and Concentrations Using LDV Techniques," *Proc. of the Dynamic Flow Conference*, Marseille, France (1978).

Fristram, R. M., Jones, A. R., Schwar, M. J. R. and Weinberg, F. J., "Particle Sizing by Interference Fringes and Signal Coherence in Doppler Velocimetry," *Faraday Symposia Chem. Soc.*, **7**, 183 (1973).

Goodman, J. W., *Introduction to Fourier Optics*, McGraw-Hill (1968).

Hacker, D. S. and Hussein, F. D., "The Application of a Laser Schlieren Technique to the Study of Single Bubble Dynamics," *Ind. Eng. Chem. Fund.*, **17**(4), 277 (1978).

Lee, S. L., and Srinivasan, J., "Measurement of Local Size and Velocity Probability Density Distributions in Two Phase Suspension Flows by Laser Doppler Techniques," *Int. J. Multiphase Flow*, **4**, 141 (1978).

Papoulis, A., "Probability, Random Variables and Stochastic Processes," Chapter 16, McGraw-Hill, New York (1965).

Rayleigh, Lord, "On the Manufacture and Theory of Diffraction Grating," *Phil. Mag.*, **11**, 196 (1881).

White, E. T., and Beardmore, R. H., "Velocity of Rise of Cylindrical Air Bubbles Through Liquids Contained in Vertical Tubes," *Chem. Eng. Sci.*, **17**, 351 (1962).

Wigley, E., "The Sizing of Large Droplets by Laser Anemometry," *UKAEA Report* AERE-R8771 (1977).

Manuscript received March 3, 1980; revision received June 6, and accepted June 17, 1980.

R & D NOTES

Hydrogen Permeation through Nickel in Gas and Liquid Phase

H. B. GALA, M. KARA, S. SUNG, S. H. CHIANG, and G. E. KLINZING

Chemical and Petroleum Engineering Dept.
University of Pittsburgh
Pittsburgh, PA 15261

Hydrogen has great importance today in the energy conversion and utilization field. The behavior of hydrogen with some metals is indeed unique showing structural decomposition of hydrogen molecule. This unique property of hydrogen can be utilized in developing a device for measuring hydrogen partial pressure, in situ. Nickel is ideally suited for developing such a tool (Gala, 1979). Many workers have studied the motion of

0001-1541-81-3386-0160-$02.00.